J. Fluid Mech. (1976), *vol.* 75, *part* 2, *pp.* 209–231
Printed in Great Britain

A comparison of the wake structure of a stationary and oscillating bluff body, using a conditional averaging technique

By M. E. DAVIES
Department of Aeronautics, Imperial College, London†

(Received 26 November 1975)

A conditional averaging technique to extract the underlying vortex pattern from a turbulent bluff body wake is described. Ensemble averages of wake velocities are developed on the basis of a reference phase position, determined from the outer flow irrotational fluctuations. The method is applied to the wakes of a stationary and oscillating D-shape cylinder, where, in the latter case, the vortex shedding is locked to the frequency of body movement. Direct comparisons of average circulation and vortex street spacings are obtained and these demonstrate the significant change in wake structure that accompanies and sustains vortex-induced vibrations. It is observed in both conditions that only 25 % of the estimated shed vorticity is found in the fully developed wake. In addition the analysis produces profiles of vorticity and velocity in an 'average vortex cycle'. A model, developed to help interpret these results, suggests that a good representation of an average wake situation is obtained by the addition of considerable mean shear to a street of finite area axisymmetric vortices.

1. Introduction

It is well known (e.g. Ferguson & Parkinson 1967) that bluff bodies which regularly shed spanwise organized vortices may be excited into oscillation by the fluctuating side forces that such vortices produce. In general the actual response to the wake forcing is a complex fluid–elastic process which depends on the dynamic properties of the body (natural frequency, damping, etc.), and on the influence its movement has on the wake itself. This interaction has been modelled by Hartlen & Currie (1970), using a nonlinear 'Van der Pol type' oscillator for the lift forces induced by the self-excited wake fluctuations, coupled to a body represented by a simple second-order linear behaviour. Although remarkably successful in describing the character of the interaction, this analogue does not provide a direct insight into the physical processes involved and it remains necessary to conduct complementary experimental investigations to determine the nature of the fluid phenomena.

The experiments of Feng (1968) demonstrate the effect of damping on the

† Present address: Division of Maritime Science, National Physical Laboratory, Teddington, Middlesex, England.

amplitude response of circular and D-shape cylinders and show the resonance that develops when the vortex shedding frequency f_s is close to the natural frequency f_n of the body. As the reduced velocity U_n is increased the oscillation amplitude continues to build up through $U_n = 1/S$ to a maximum resonance at some higher value of U_n ($U_n = U_0/f_n d$, where U_0 is the free-stream velocity, d is a representative body dimension and $S = f_s d/U_0$ is the Strouhal number of the stationary body). In the resonant condition it has been found (Toebes 1967; Koopmann 1967) that the spanwise correlation of wake velocity fluctuations is improved and also, at low Reynolds number, Griffin (1972*a*) suggests that vortex strengths are increased.

The aim of the work reported here was to examine the detailed structure of the turbulent wake of a stationary and oscillating body. A convenient method of examining the resonant wake–body interaction is to oscillate the cylinder mechanically and it has been demonstrated by Griffin (1972*b*) that this can produce a certain equivalence to a naturally excited situation. Such was the method used in these experiments to create a wake wherein the vortex shedding was synchronized to the simple harmonic oscillations of the body.

2. Choice of bluff body and resonant condition

It has been shown (Davies 1975) that the precise nature of an oscillating body–wake interaction is dependent on the geometry of that body, the afterbody shape having a strong influence on the behaviour of the near wake. Different cylinder shapes are excited to a varying degree by their vortex wakes and not all mechanically oscillated bodies are able to synchronize their wake fluctuations completely. A bluff body which can produce a complete frequency locking of vortex shedding to its own movement is a D-shape cylinder, i.e. a cylinder with a uniform cross-section comprising a flat face normal to the oncoming stream and a rearward facing semicircle. This simple shape also has the advantage that any Reynolds number sensitivity would be expected to be small because of its sharp edges and was chosen for the experiments described here. It was confirmed that the stationary-body base pressure and Strouhal number were invariant in the range covered, which was from 7×10^3 to 4×10^4, based on the semicircle diameter. This cross-flow dimension d was 50 mm and the cylinder spanned a 0·91 m square low turbulence wind tunnel, on its centre-line. Light end plates were rigidly attached to the model, giving an effective aspect ratio of 15·8:1, and this produced a good degree of spanwise uniformity of the mean base pressure. Although no further spanwise measurements were made, it was observed on a similar sharp-edged model of the same aspect ratio but with a shallower afterbody that the vortex filaments were aligned parallel to the cylinder in both stationary and oscillating conditions.

The cylinder was oscillated by a scotch-yoke mechanism situated wholly outside the tunnel, which produced a maximum total vertical displacement $2a$ of $0{\cdot}6d$. It was found that a convenient working arrangement was $2a/d = 0{\cdot}4$, and figure 1 shows the resulting wake periodicity and base pressure behaviour

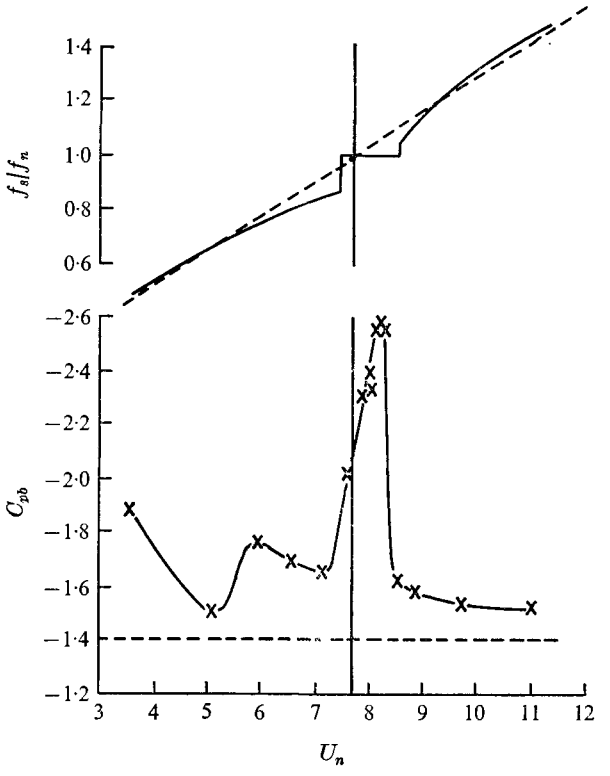

FIGURE 1. Variation of shedding frequency and base pressure with free-stream velocity, for a D-shape cylinder. – – – –, stationary; —×—, oscillating ($2a/d$ = 0·4).

when the tunnel velocity was increased, with the cylinder oscillating with this amplitude at a constant frequency f_n. The shedding is observed to be locked to the frequency f_n over a range of 0·96–1·10 of the resonant velocity $U_n = 1/S$ (where S is the stationary-body Strouhal number), but it is noted that the base pressure coefficient is not constant in this region. Figure 2 displays spectra of velocity fluctuations for a stationary and oscillating case, where, for the latter, U_n = 8·0. The streamwise fluctuations were measured $6d$ behind the cylinder and $3{\cdot}75d$ out from the centre-line and figure 2(*b*), with a single sharp spectral peak, shows how completely the wake oscillations were locked to the frequency of body movement, the displacement spectrum of which is shown in figure 2(*c*). In this resonant condition the base pressure coefficient was reduced to −2·39, an increase in base suction of 70 % compared with the stationary-cylinder value. This indication of greatly increased drag is substantiated by the comparison of mean velocity defects plotted in figure 3, though it is interesting to note that the overall wake width is no larger in the oscillating case, in spite of the lateral movement of the body that generates it. At low Reynolds number Koopmann (1967) inferred from flow-visualization studies an apparent decrease in lateral vortex spacing in the resonant wake of an oscillating circular cylinder and it might be conjectured that a similar phenomenon occurs in these turbulent wakes.

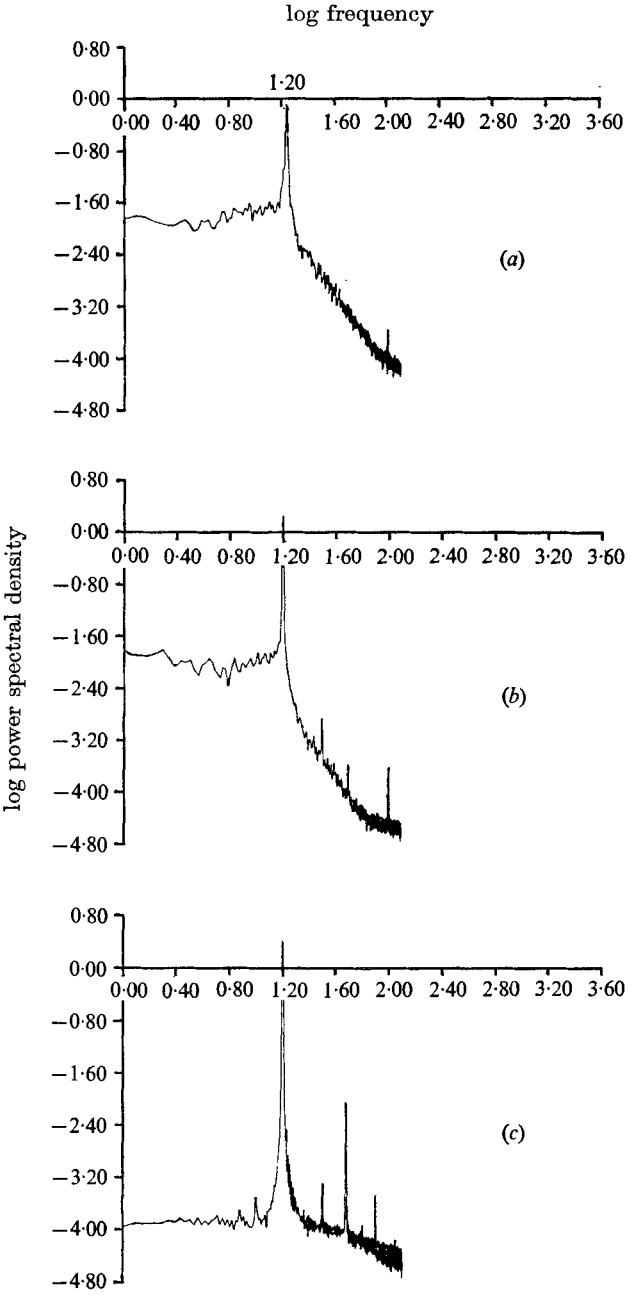

FIGURE 2. Spectra of u velocity fluctuations at $(x, y) = (6, 3{\cdot}75)$ in the wake of (*a*) a stationary and (*b*) an oscillating ($2a/d = 0{\cdot}4$, $U_n = 8{\cdot}06$) D-shape cylinder and (*c*) spectrum of cylinder displacement.

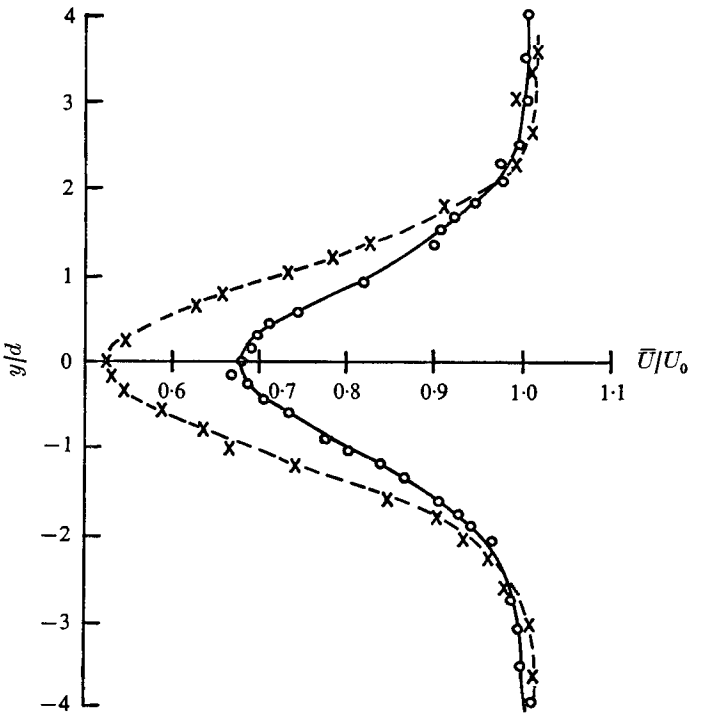

FIGURE 3. Time-mean wake profiles at $8d$ behind a D-shape cylinder. —○—, stationary; – –×– –, 'locked' oscillating ($2a/d = 0{\cdot}4$, $U_n = 8{\cdot}0$).

The subsequent sections describe a method of extracting a direct measure of average vortex spacing, strength and structure from a turbulent wake flow, in order that these ideas can be explored further.

3. A conditional averaging technique to extract the underlying near-periodic elements from a turbulent vortex wake

An instantaneous measurement of the velocities in a turbulent wake proves difficult to interpret because of the presence of large amplitude random fluctuations. Figure 4, for example, shows the velocity trace from a hot-wire anemometer at point (*b*) in the wake of a two-dimensional flat plate and demonstrates the strong influence of the turbulence. By contrast, outside the wake (at position (*a*)), the hot wire measures the recognizably periodic irrotational fluctuations induced by the coherent wake structure. These oscillations are, of course, strongly related to the vortices in the wake and, thus, indicate their passage downstream through the plane of the measuring station. The principle of the ensemble averaging procedure was to use the irrotational 'sensor' signal to provide a reference phase angle to which the wake velocity could be related. The sensor reference was taken to be a maximum in the u velocity (streamwise) oscillations. Consider then a wake velocity $W(t)$ and a sensor velocity $S(t)$ measured at points separated only in the transverse (y) direction. In practice both signals were digitized and

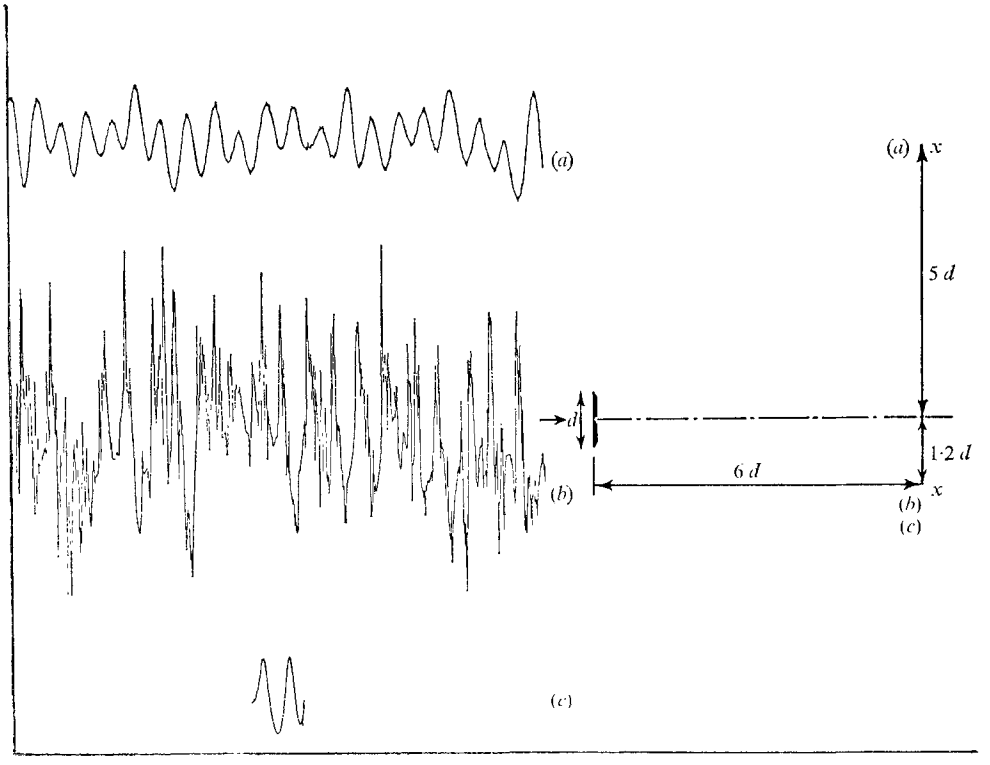

FIGURE 4. Hot-wire signals recorded $6d$ behind a flat plate normal to a uniform stream. (*a*) Sensor in irrotational flow. (*b*) Wake signal. (*c*) Averaged signal. x, hot-wire positions.

the resultant time series W_i and S_i were recorded on digital magnetic tape for subsequent analysis.

Examination of a length of recording reveals the series S_i to have N maxima, say, occurring at $i = m(j)$, $j = 1, \ldots, N$. The simultaneous wake velocity is given by $W_{i=m(j)}$ and, therefore, an average velocity at this particular time in the vortex wake cycle is given by

$$\overline{W}_m = \frac{1}{N} \sum_{j=1}^{N} W_{m(j)}. \tag{3.1}$$

By definition the mean of the random fluctuations at this phase position is zero and, thus, if N is sufficiently large to provide a good statistical estimate of the mean, the turbulence is removed and the underlying average is produced. (For a Gaussian random variable with standard deviation $0{\cdot}3\mu$, 4000 estimates yield an error of less than $\pm 1\,\%$ of μ, the mean, with 95 % probability.) Clearly (3.1) can be extended to a segment T of the vortex cycle by taking elements of W_i adjacent to $i = m(j)$. Thus

$$[\overline{W}_i]_T = \frac{1}{N} \sum_{j=1}^{N} [W_i]_j, \tag{3.2}$$

where $[\overline{W}_i]_T$ is the averaged segment of length T and $[W_i]_j$ is the measured series of velocities about the jth maximum, i.e. $m(j) - \frac{1}{2}T \leqslant i \leqslant m(j) + \frac{1}{2}T$. To reveal

a complete wake cycle, T should equal the period of vortex shedding, and an estimate of its magnitude at any time is given by $m(j)-m(j-1)$. However, owing to the possible variability of T, this can produce a decreasing number of samples as the edges of the segment are approached. To improve the resolution at the ends of the cycle, therefore, the segment was extended to $\pm T$. The result of averaging the wake signal shown in figure 4(*b*) on the basis of sensor (*a*) is displayed as figure 4(*c*). Two cycles are produced with an effective repetition of the approximate half-cycle on either side of the central segment.

In assessing the merit of this technique it is important to realize that the same average could not be obtained by band-pass filtering about the shedding frequency. Such a process would exclude the second-harmonic fluctuations of u velocity that develop in the wake centre and would also fail to remove that part of the turbulence spectrum within the filtering band. Neither is the sampling strictly periodic, since it allows for variability in the shedding process, though it is admitted that certain irregularities in the wake may reduce the effectiveness of the averaging. A particularly large adjacent vortex, for example, may modify the position of the local sensor maximum relative to the phase of its associated wake cycle. Also the pattern at the edges of the cycle will become smeared if the period is too variable. These considerations are, however, the essence of the averaging process, underlining the fact that the notion of a typical or mean vortex pattern is only useful when the variation in its periodic character (not the turbulence) is small.

A complete average velocity field may be obtained by traversing a cross-wire across the wake to measure simultaneously the u and v velocities.

4. Application and results of conditional averaging

It has been observed that some consideration of the basic vortex shedding pattern is necessary before applying the technique described in §3. Figure 2 showed the periodic velocity fluctuations induced by the wakes of a stationary and synchronized oscillating cylinder to be well 'tuned' in a narrow frequency band. Additionally, figure 5 displays the velocity signals that correspond to figures 2(*a*) and (*b*) and these demonstrate the degree of amplitude modulation that exists in these situations. The stationary-body shedding is less regular than that produced by the oscillating cylinder, but it is not possible to determine whether this is due to varying vortex strength, position or a combination of both. In this respect it should be noted that the conditional ensemble average produces an arithmetic mean of the induced velocity field, though not necessarily of the other wake features. The low-frequency modulation is seen from the velocity spectra to be distributed over a range of frequencies. These oscillations are in-phase across the wake and may be interpreted as slow pulsations of the vortex formation region.

Complete lateral traverses of both wakes were made at $8d$ downstream of the body. The u and v fluctuations were recorded at 28 lateral positions in the case of the stationary cylinder and 27 positions in the oscillating situation. These results for a vortex shedding cycle have been combined to form plots of stream-

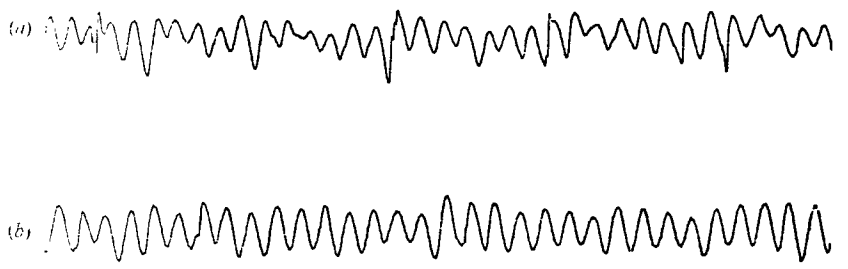

FIGURE 5. Hot-wire velocity traces outside the wake of a D-shape cylinder. (*a*) Stationary body. (*b*) 'Locked' oscillating condition ($2a/d = 0{\cdot}4$, $U_n = 8$).

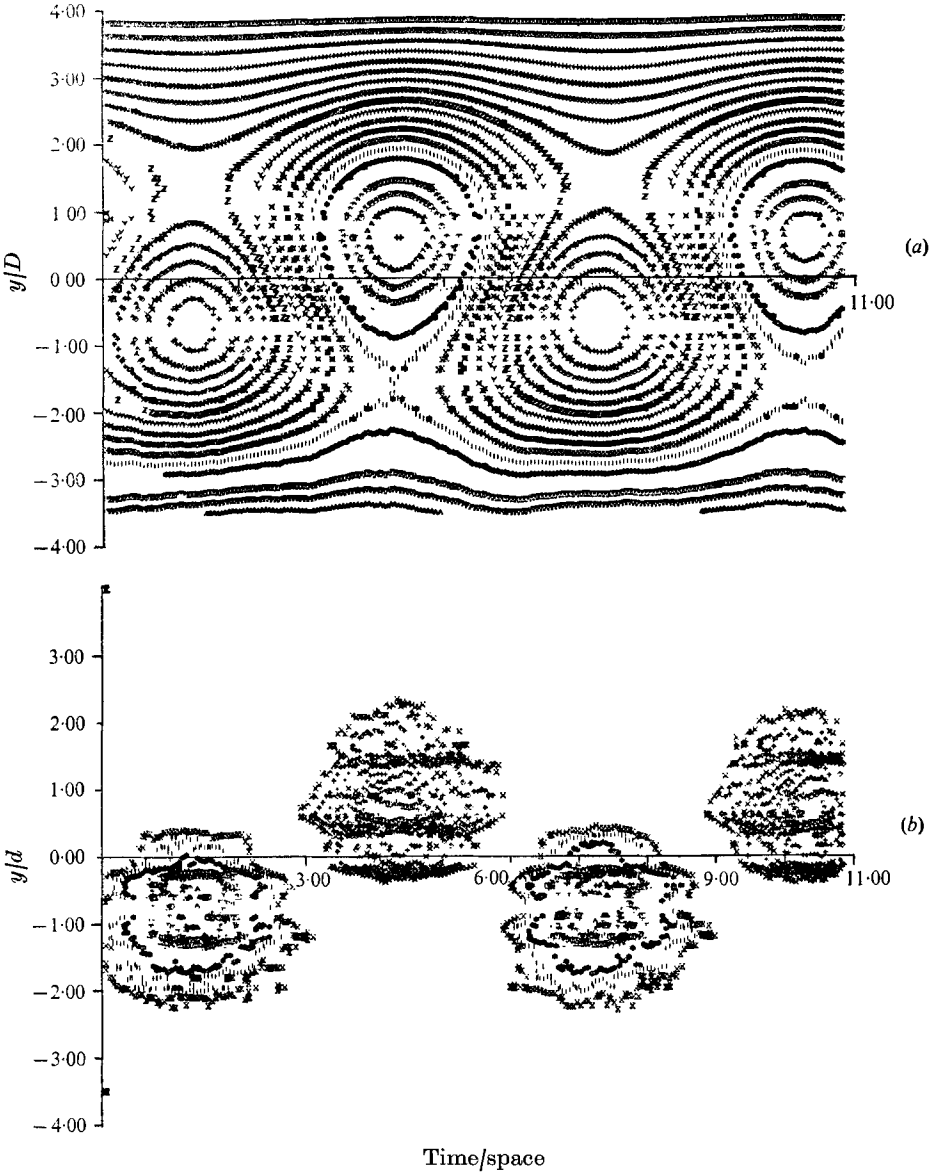

FIGURE 6. The vortex wake around $x = 8d$ behind a stationary D-shape cylinder. A convection velocity of $0{\cdot}8U_0$ has been removed to make the vortex centres stationary. (*a*) Streamlines. (*b*) Vorticity contours (lowest 20 % removed). Flow direction from right to left.

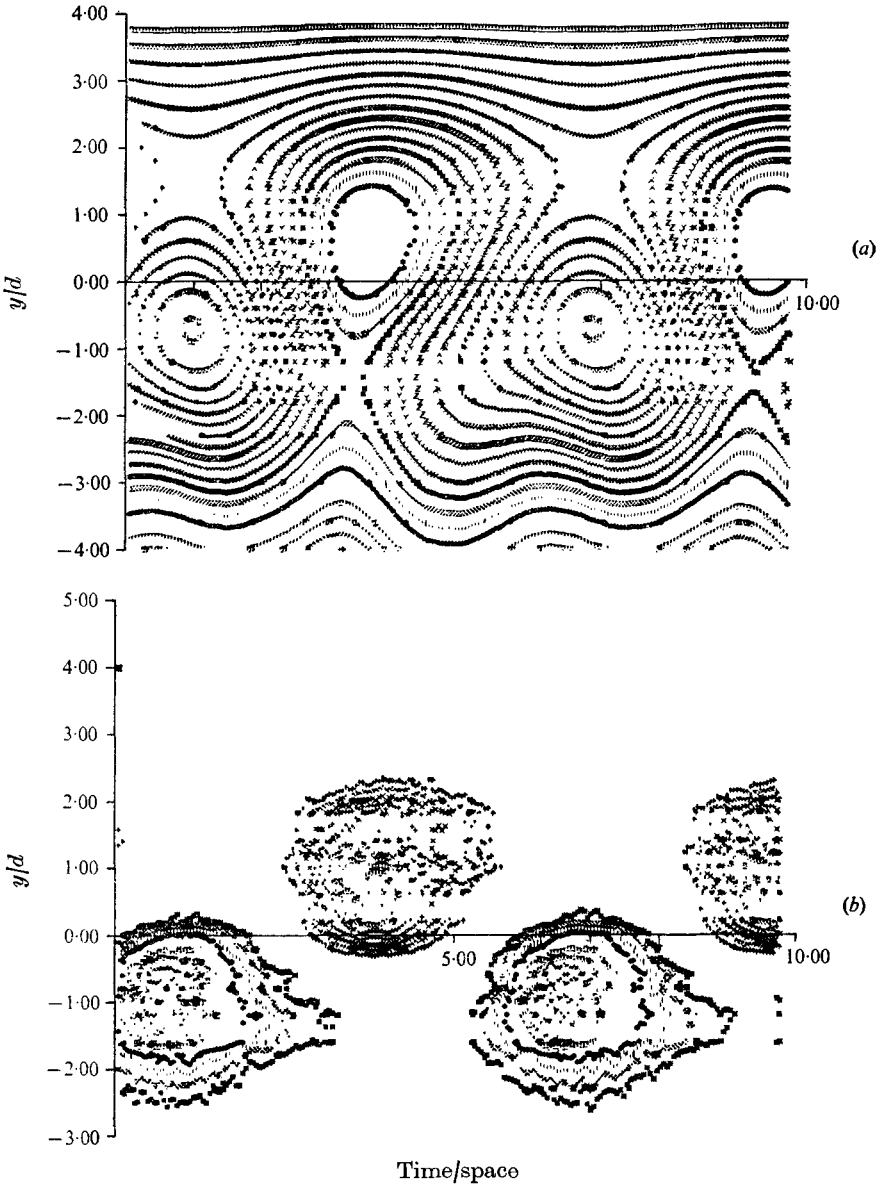

FIGURE 7. The vortex wake around $x = 8d$ behind an oscillating D-shape cylinder. A convection velocity of $0{\cdot}72U_0$ has been removed to make the vortex centres stationary ($2a/d = 0{\cdot}4$, $U_n = 8{\cdot}0$, $C_{pb} = -2{\cdot}39$). (*a*) Streamlines. (*b*) Vorticity contours (lowest 20 % removed). Flow direction from right to left.

lines and vorticity contours and are shown in figures 6 and 7. Strictly the velocity field (u, v) is a distribution in the t, y plane at some x. However, with the assumption of a frozen vortex pattern, convected with velocity U_c, x space has been related to t by $x = U_c t$. The estimation of U_c, the downstream convection speed of vortex centres, is itself a problem and is discussed more fully by Davies (1975). The values used in the two cases under consideration were $0{\cdot}8U_0$ and $0{\cdot}72U_0$ for

the stationary and oscillating conditions, respectively. They were measured by means of two hot wires with considerable longitudinal separation (around $4d$) about the $x = 8d$ position. The stream function was evaluated as

$$\psi(x,y) = \psi_0 + \int (u\,dy - v\,dx),$$

where ψ_0 was defined as zero on an outer free-stream streamline, and an estimate of the vorticity was obtained from $\omega(x,y) = \partial v/\partial x - \partial u/\partial y$. Figure 6 shows an averaged vortex street arrangement composed of fairly circular vortices. This does not mean, however, that each individual vortex is of this shape; in fact, it is strongly argued by Davies (1975), from other evidence, that the wake consists of non-circular vortex clouds which distort and rotate as they are convected downstream. Thus the circular pattern may arise from averaging over vortices which arrive at the measuring position with random orientation. The streamlines of figure 7, by contrast, show some departure from axial symmetry and this could be indicative of significant differences in the wake development. Although there is evidence (Davies 1975) that the vortex clouds still rotate as they convect downstream, it is suggested that the vortex production process is much more closely controlled when it is driven by the oscillating cylinder. This is supported by the regular trace of figure 5(*b*) and could lead to vortices arriving at the measuring location with a much less variable orientation. In addition, although it is generally true that the averaging will tend to remove, rather than accentuate, irregularities, it must be concluded that the waviness of the outer streamlines in the lower part of the wake is due to accumulated error in the integration process across the wake, from the reference streamline at $y = +4d$.

Figures 6 and 7 give a general impression of the vortex street geometry, but a rather less general representation of the results is necessary to quantify certain of the features. The vortex centres in figure 6 are located at approximately $\pm 0{\cdot}6d$ and, from an examination of the distribution with x along $y/d = 0{\cdot}6$, the maximum was found at $4{\cdot}35d$ relative to the origin shown. Through $y/d = -0{\cdot}6$ the oppositely signed vorticity is revealed to peak on either side of the upper maximum, suggesting a longitudinal vortex separation of around $6{\cdot}05d$, which is close to the value of $6{\cdot}15d$ obtained from the shedding period and convection velocity, i.e. from $l = U_c/f_s$. Figures 8 and 9 plot the variation of averaged vorticity and velocity through the upper vortex centre. Figure 8 confirms the centre to be near $y/d = 0{\cdot}6$ and figure 9 establishes the value as about 0·63 (i.e. $b/d = 1{\cdot}26$, where b is the lateral vortex spacing) by matching with the independently measured convection velocity.

By the same analysis the synchronized wake yields a value of $5{\cdot}95d$ for the longitudinal separation, which is consistent with that calculated from $l = U_c/f_s$. The lateral spacing is seen to be slightly greater than for the stationary body, figures 7, 10 and 11 suggesting a value of $b/d = 1{\cdot}5$.

A third parameter of the vortex street which can be estimated from these results is the average strength (circulation) of an individual vortex. The integral $\int_S \mathbf{u}.d\mathbf{s}$ was calculated around a contour which enclosed a vortex and passed through points of zero vorticity. The results, summarized in table 1, show an

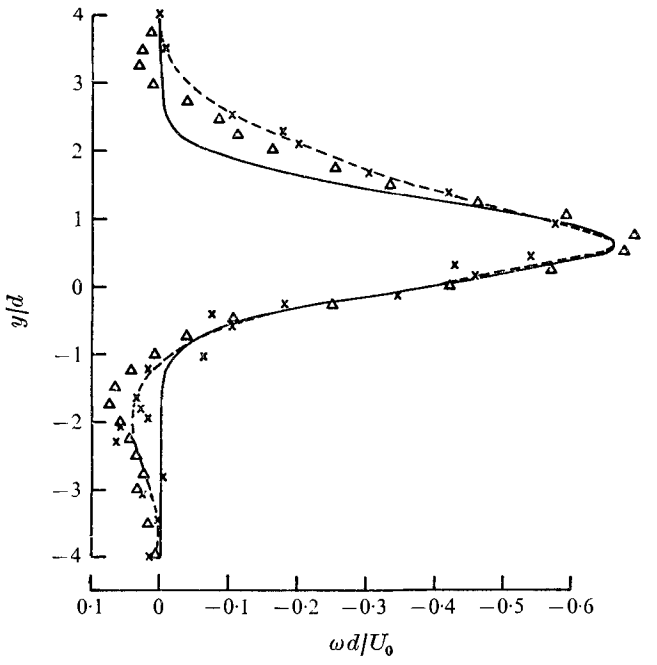

FIGURE 8. Distribution of vorticity through a vortex centre at $x = 8d$ behind a stationary D-shape cylinder. – – × – –, experiment; ——, model prediction ($\Gamma/U_0 d = 1{\cdot}66$, $R_0/d = 1{\cdot}0$); △, modified model.

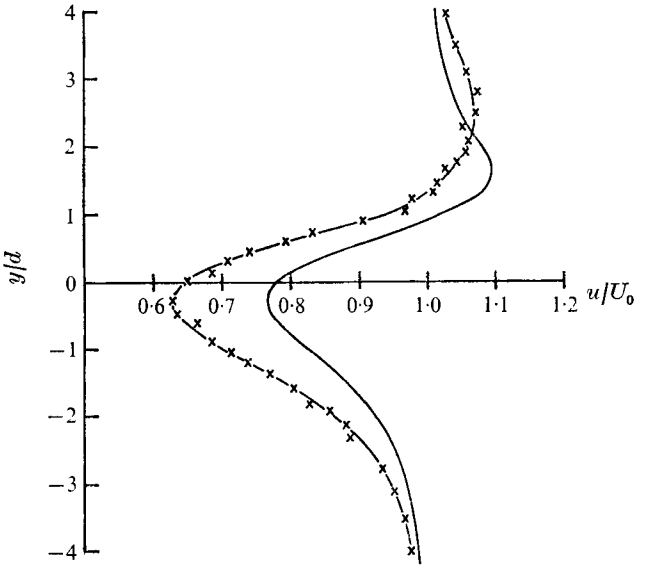

FIGURE 9. Stationary D-shape cylinder wake at $x = 8d$. — × —, average velocity profile through a vortex centre; ——, model prediction ($\Gamma/U_0 d = 1{\cdot}66$, $R_0/d = 1{\cdot}0$, $b/l = 0{\cdot}21$, $b/d = 1{\cdot}26$, $l/d = 6{\cdot}1$).

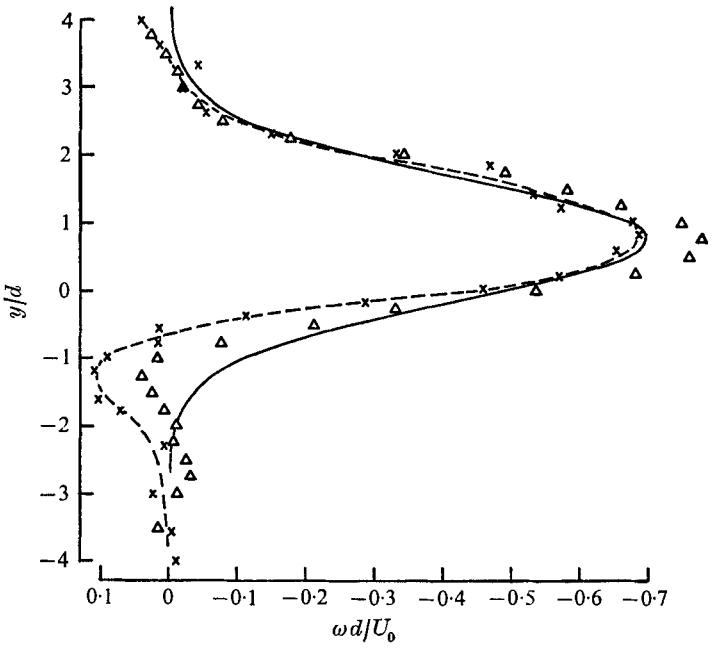

FIGURE 10. Distribution of vorticity through a vortex centre at $x = 8d$ behind an oscillating D-shape cylinder ($2a/d = 0{\cdot}4$, $U_a = 8$, $C_{pb} = -2{\cdot}39$). – – × – –, experiment; ——, model prediction ($\Gamma/U_0 d = 3{\cdot}67$, $R_0/d = 1{\cdot}45$); △, modified model.

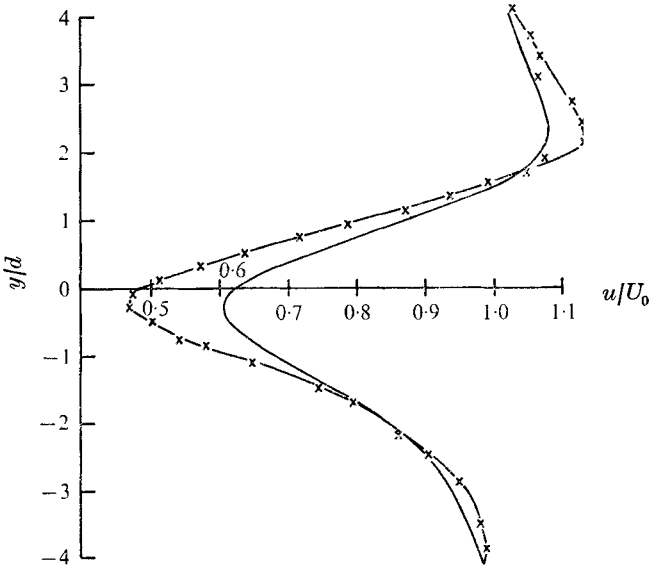

FIGURE 11. Oscillating D-shape cylinder wake at $x = 8d$. — × —, average velocity profile through a vortex centre ($2a/d = 0{\cdot}4$, $U = 8$); ——, model prediction ($\Gamma/U_0 d = 3{\cdot}67$, $R_0/d = 1{\cdot}45$, $b/l = 0{\cdot}25$, $b/d = 1{\cdot}5$, $l/d = 5{\cdot}95$).

	Stationary D-shape cylinder	Synchronized oscillating cylinder
C_{pb}	−1·4	−2·39
U_c	0·8	0·72
l/d	6·1	5·95
b/d	1·26	1·5
b/l	0·21	0·25
$\Gamma/U_0 d$	2·39	3·24
α	26%	24%

TABLE 1. Comparison of overall wake parameters due to a stationary and 'synchronized' oscillating D-shape cylinder

increase of 35 % in the circulation Γ of vortices shed from the oscillating cylinder, compared with those in the wake of a stationary body. This increase in vortex strength is important in terms of self-excited oscillations, since it implies that a primary mechanism for increasing the fluctuating side forces on the body is provided by a changed sectional wake structure and this effect is additional to any increased spanwise correlation. Evidence for a modified vortex development process, in the oscillating case, has been given by a flow-visualization film which clearly shows that the roll-up of the separated shear layers takes place much closer to the rear face of the body. This could be consistent with the fact that the roll-up of a shear layer is dependent on its vorticity density (Kaden 1931), and should therefore be related to the total vorticity contained in the fully developed wake. The increase in vortex strength could, of course, be due to less destruction in the shear-layer interaction across the wake (Gerrard 1966), rather than as a result of more vorticity being shed into the shear layers, and this aspect bears further investigation.

In considering the net circulation remaining in a vortex wake, Fage & Johansen (1927) and Roshko (1954) suggested an estimate of the total shed by a body could be calculated from the value of the mean base pressure. A measure of the rate of production of circulation at each separation point is given by $d\Gamma/dt = \frac{1}{2}U_b^2(t)$, where U_b is the velocity at the edge of the boundary layer. On the assumption of a constant time mean pressure across the shear layers, the average velocity $\overline{U}_b$ is approximated by kU_0, where $k^2 = 1 - C_{pb}$. Thus the total circulation of each sign produced in a vortex shedding cycle T is

$$\Gamma_T = \tfrac{1}{2}k^2 U_0^2 T(1 + \overline{(u'/kU_0)^2}), \tag{4.1}$$

where u' is the fluctuation of U_b about kU_0. For a circular cylinder at Reynolds numbers around 10^5, Dwyer & McCroskey (1973) show $\overline{(u'/kU_0)^2}$ to be approximately 0·02 and it is generally considered that this contribution to Γ_T can be neglected. Thus from a non-dimensionalized measurement of vortex strength in the downstream wake, $\Gamma_m = \Gamma/U_0 d$, the fractional circulation remaining can be expressed as

$$\alpha = 2S\Gamma_m/(1 - C_{pb}). \tag{4.2}$$

Table 1 shows for the two situations under consideration that only a quarter of the shed vorticity is found in the developed vortex street at $x/d = 8$. That the

fractional destruction is apparently the same supports the contention that more circulation is produced by the oscillating body. It is argued (Davies 1975) that the body movement provides an additional vorticity input, which is related to its acceleration. This forced input adds to and modifies the normal wake-generated fluctuations, in the manner described by the nonlinear oscillator models. In the synchronous region the phase of the vortex development is controlled by the body movement, such that the additional vorticity produced reinforces the currently growing vortex. In this way shear layers of a high vorticity density may develop, producing strong vortices and a velocity field in the near wake which helps the vortex clouds resist downstream convection by the free stream and promotes growth closer to the rear face of the body.

Although the measure of shed vorticity given by (4.1) provides a useful means of comparing results, it should be emphasized that it is a definition that needs careful interpretation and this point is raised to discuss further the question of vorticity destruction in the developing wake. The fluctuating pressure measurements of Novak & Tanaka (1975) for an oscillating circular cylinder with synchronized vortex shedding indicate that not only is the average vorticity production enhanced (i.e. k increases), but also the process is more asymmetric between the separation points (i.e. $\overline{(u'/kU_0)^2}$ increases) in comparison with the corresponding stationary case. This was borne out by flow visualization in the case of the oscillating D-shape body, where the growing vortex appeared to develop with less interference from the opposite shear layer. Owing to its proximity to the rear surface there did, in fact, seem to be a strong interaction with the body, with the possible production of secondary vorticity at this boundary. Such a mechanism of cancellation of vorticity at source might explain the similar total wake circulation loss in the two cases, in spite of a changed mixing process, and it is wondered, therefore, whether more emphasis should not be placed on the role of the cylinder base in destroying vorticity produced by its front face. This feature is included in the description of vortex shedding given by Gerrard (1966), although most attention is directed to the cross-wake cancellation mechanism. Sarpkaya (1975) also discusses the same question in relation to his numerical modelling of a flat-plate wake. Both he and Clements (1973) find little circulation loss ($\alpha \sim 0{\cdot}85$) and short vortex formation distances in their computational experiments and it seems possible that both methods underestimate the effect of the rear surface of the body.

A value of 0·85 for α is particularly high in comparison with the values around 0·25 presented here and also significantly greater than the estimates of 0·6 (Fage & Johansen 1927), 0·43 (Roshko 1954) and 0·30 (Bloor & Gerrard 1966, assuming $\Gamma/\pi U_0 d = 0{\cdot}5$, $C_{pb} = -1{\cdot}10$, $S = 0{\cdot}20$). In support of the present results, it is shown in the next section that estimates of vortex strength inferred from a vortex street model can be very dependent on the analysis employed.

5. Matching of conditionally averaged results with a wake model

5.1. *The model*

A number of previous investigators (Fage & Johansen 1927; Timme 1957; Schaeffer & Eskinazi 1959; Berger 1964; Bloor & Gerrard 1966; Griffin 1972*a*) have appealed to vortex street models to help interpret their measurements in bluff body wakes. The present results, however, give a direct estimate of the structure of the wake of a D-shape cylinder and this provides an opportunity to compare in detail the characteristics of the measured wake with those of a simple model.

Schaefer & Eskinazi considered a finite vortex street and predicted certain asymmetric features of the velocity fluctuations, close to the body. By comparison, at eight diameters behind the D-shape body, the averaged traces were much more symmetric and it seemed that an infinite-street approximation would be more valid. It was decided to use a simple Kármán vortex street arrangement of point vortices, with certain singularities replaced by some axisymmetric finite-area vortex structure. The likely character of a turbulent vortex is a subject that has engaged a number of authors, especially in connexion with aircraft trailing vortices. Saffman (1973) adopted a scaling approach similar to that employed for turbulent boundary layers, to predict the circulation variation. Like Hoffman & Joubert (1963), Saffman suggested an outer core with a logarithmic increase in overall circulation and an inner core (including an inner viscous core) with 'solid-body rotation'. Bloor & Gerrard (1966) considered Hoffman & Joubert's model and found support for their outer core representation, but concluded, indirectly, that the familiar exponential viscous vortex provided a better inner core description. Figures 8 and 10 show an exponential viscous vortex model matched to the measured profiles of vorticity. Clearly the distribution around the vortex centre is better described this way than by the constant vorticity of the 'solid-body rotation' model, though the outer regions are less well matched. However, on further consideration it was not found that the inverse-square vorticity decay of an outer logarithmic circulation increase was significantly better, so a simple viscous vortex representation was decided upon as the basic framework of a vortex wake model.

The viscous vortex profile referred to is that obtained from the solution for a line vortex diffusing under the action of viscosity, viz.

$$u_\theta = (\Gamma/2\pi r)\,[1-\exp(-r^2/4\nu t)], \tag{5.1}$$

where r is the radial distance from the position of the line vortex of strength Γ at time $t = 0$. The velocity described by (5.1) is zero at the vortex centre and rises to a maximum at a radius R_0, which is a function of time. The vortices used in the model were chosen to be described completely by their strength Γ and core radius R_0 (the model had no time dependence), both of which were parameters of the matching procedure.

Thus the viscous vortex produces the following velocity and vorticity variations about its centre:

$$u_\theta = (\Gamma/2\pi r)\,[1-\exp(-1{\cdot}26(r/R_0)^2)], \tag{5.2}$$

$$\omega = (1{\cdot}26\Gamma/\pi R_0^2)\exp[-1{\cdot}26(r/R_0)^2]. \tag{5.3}$$

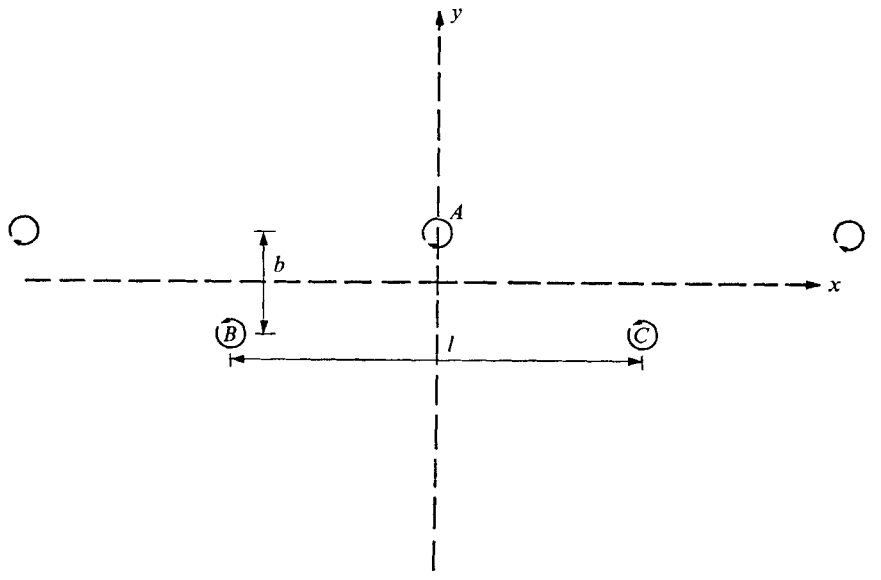

FIGURE 12. Vortex street arrangement showing replacement vortices A, B and C.

As the far-field influence given by (5.2) is that of a potential vortex, it was only necessary to replace point vortices in the Kármán street near regions of interest. It is recognized, of course, that (5.3) is a solution of

$$\frac{\partial \omega}{\partial t} = \nu \left(\frac{\partial^2 \omega}{\partial r^2} + \frac{1}{r} \frac{\partial \omega}{\partial r} \right)$$

and that this particular axisymmetric form of the vorticity equation does not apply in a wake, where one vortex exists in the strain field of other vortices. The superposition of these profiles is intended merely as a means of describing a first approximation to an average vortex street.

Three point vortices in an infinite street were removed and replaced by vortex structures described by (5.2) and (5.3). The resulting complex velocity $v = u + iv$ is given, in the complex plane $z = x + iy$, by

$$\bar{v} = \frac{i\Gamma}{2\pi} \left\{ \frac{\pi}{l} \cot \frac{\pi}{l} (z - z_A) - \frac{\pi}{l} \cot \pi (z - z_C) - \frac{1}{z - z_A} + \frac{1}{z - z_B} + \frac{1}{z - z_C} + \alpha_A - \alpha_B - \alpha_C \right\}, \tag{5.4}$$

where Γ is the total circulation of each vortex in the street, A, B, and C identify the three viscous vortex positions (figure 12), b and l are the lateral and longitudinal vortex separations,

$$\begin{aligned}
z_A &= \tfrac{1}{2} ib, \quad r_A^2 = x^2 + (y - \tfrac{1}{2} b)^2, \\
z_B &= -\tfrac{1}{2} l - \tfrac{1}{2} ib, \quad r_B^2 = (x + \tfrac{1}{2} l)^2 + (y + \tfrac{1}{2} b)^2, \\
z_C &= \tfrac{1}{2} l - \tfrac{1}{2} ib, \quad r_C^2 = (x - \tfrac{1}{2} l)^2 + (y + \tfrac{1}{2} b)^2, \\
\alpha_J &= [(1 - \exp(-1{\cdot}26 (r_J / R_0)^2)) (\bar{z} - \bar{z}_J)] / r_J^2,
\end{aligned}$$

for $J = A, B, C$; an overbar represents the complex conjugate.

It is considered that the insertion of the vortices at A, B and C provides a representation of the velocity field in $-\frac{1}{2}l \leqslant x \leqslant \frac{1}{2}l$ and assumed that this wake cycle repeats throughout space (or time, if one considers the vortex street convecting past a fixed point). The cyclic repetition allows a Fourier decomposition to be made, the transform of the u velocity fluctuation being simply

$$\mathscr{F}(\lambda) = \frac{1}{l} \sum_{N=-\infty}^{\infty} \delta(\lambda - N/l) \int_{-\frac{1}{2}l}^{\frac{1}{2}l} u(x) \exp(-2\pi i x\lambda)\, dx, \tag{5.5}$$

which yields energy estimates at the fundamental and harmonic frequencies, or wavenumbers. A number of preliminary investigations (reported in Davies 1975) demonstrate the general good behaviour of the model and have brought to light some interesting features. Bloor & Gerrard observed that the peak intensity of the fundamental u velocity fluctuations did not occur at the core radius and this is predicted by the model for vortices of sufficiently large area. As the core radius is increased and the cross-wake influence increases the peak energy moves slowly inwards towards the vortex centre and, in fact, considerable fluctuations are found along the line of centres itself. That the induced velocity is not constant along this line emphasizes the fact that the vortex convection speed cannot be equated to the time-mean wake velocity at the lateral position of the vortex centre. This is demonstrated experimentally by comparing figures 3 and 9, in the region of the vortex centre, $y/d = 0{\cdot}63$ ($\overline{u}/U_0 \sim 0{\cdot}75$, $U_c/U_0 = 0{\cdot}8$).

The next step was to attempt to match the detailed wake profiles, obtained by the conditional averaging process, to those of the vortex model in order to highlight any fundamental inadequacies in this representation.

5.2. *Stationary* D*-shape cylinder*

It can be seen from (5.3) that the maximum vorticity in the viscous vortex occurs at its centre ($r = 0$), and is a function of Γ and R_0 only. It has been remarked that the maximum u velocity fluctuations occur near the core radius R_0, and this feature has been used in producing the match shown in figure 13. The values of $\Gamma/U_0 d = 1{\cdot}66$ and $R_0/d = 1$ were arrived at by seeking a good match consistent with $(1{\cdot}26\Gamma/\pi R_0^2) = \omega_{\max}$, from (5.3); where $\omega_{\max}$ was obtained from the experimental points in figure 8. A prediction of the u velocity variation through a vortex centre can now be obtained from (5.4) using the above values of Γ and R_0, plus the empirically determined spacing ratios (table 1). A comparison with the measured profile is displayed in figure 9, where a free stream has been added to the stationary arrangement drawn in figure 12. It is immediately obvious that the match is poor and, particularly, that the model underestimates the induced backflow in the centre of the wake. It can now be seen from figures 9 and 13 how various estimates of circulation may be inferred from a vortex street representation. Clearly much higher values of vortex strength would be required to satisfy completely the difference between the vortex convection speed and the free-stream velocity, using a Kármán potential street model. On the other hand the analysis of the wake fluctuations performed by Bloor & Gerrard yielded vortices compatible with the match shown in figure 13. Fage & Johansen also used a

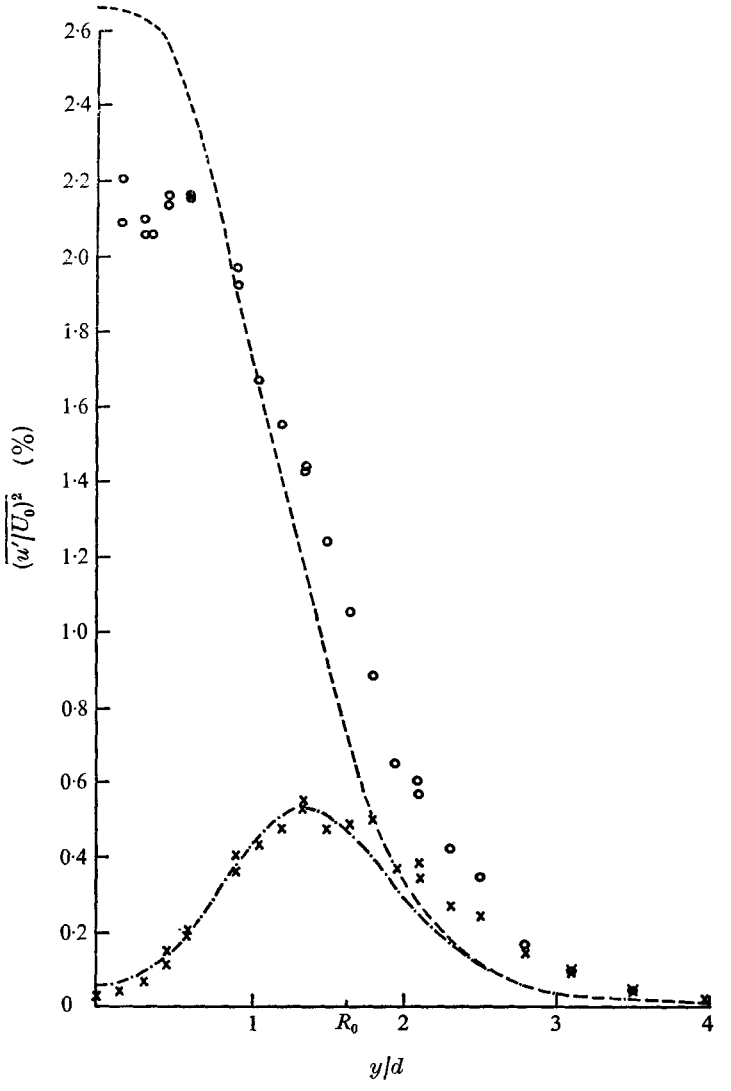

FIGURE 13. Variance of average velocity fluctuations at $x = 8d$ in the wake of a stationary D-shape cylinder. Experiment: ×, u velocity; ○, v velocity. Model predictions: —·—, u velocity; – – –, v velocity.

fluctuating velocity approach, but their measurements were made outside the wake and figure 13 reveals the need for larger circulations to match the far-field effects. It remains, however, to reconcile the various defects in the model predictions, so consider now the deficiency in the wake profile in figure 9. This is shown plotted in figure 14, together with an inversion of the same curve to simulate the velocity through the centre of a vortex on the other side of the wake. The combined picture emphasizes the symmetry of the basic curve, the mean being reasonably close to either profile. This is an interesting outcome since the addition of a mean wake defect would, of course, add no energy to the

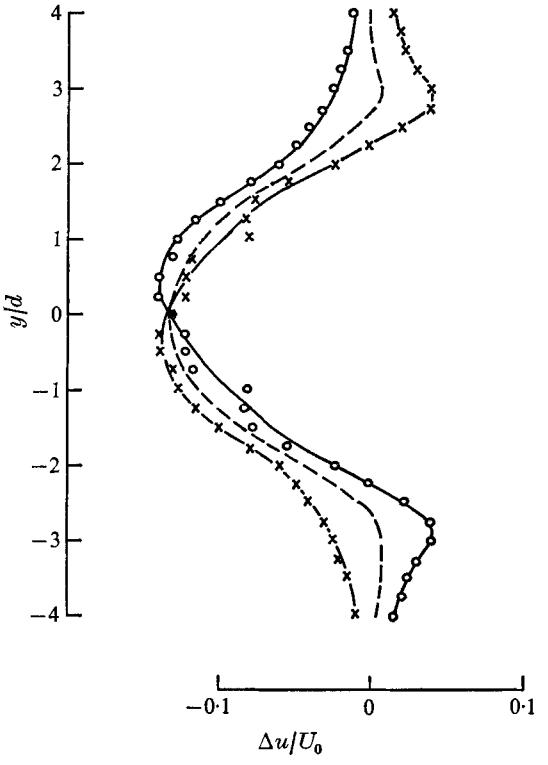

FIGURE 14. Stationary D-shape cylinder. Additional velocity required to match theoretical model with experiment. —×—, required velocity through a vortex centre; —○—, inversion of —×— profile; – – –, mean additional shear.

model prediction of figure 13. The greatest asymmetry of the defect velocity in figure 14 is around $y/d = 3$ and these fluctuations are seen to be necessary to complete the matching of the energy distribution in figure 13. It is possible that the difficulty in matching the outer wake energy and also the centre-line v fluctuations may be attributable to a smearing of the measured pattern by the variability of vortex strength and position. To substantiate the consistency of the model further, the addition of the mean shear to the basic model prediction of time-mean velocity is shown in figure 15 to produce a perfect match with the experimental points.

It now merely remains to calculate the additional vorticity contributed to the wake by this mean shear field. On the assumption of negligible mean v velocities, the contribution to the vorticity has been taken as that given by differentiating the average profile of figure 14. The resulting values have been added to the model curve in figure 8, which now demonstrates good agreement with the experimental measurements and suggests strongly that a good representation of an average vortex wake of a D-shape cylinder is given by a staggered street of circular-area vortices together with a substantial mean shear.

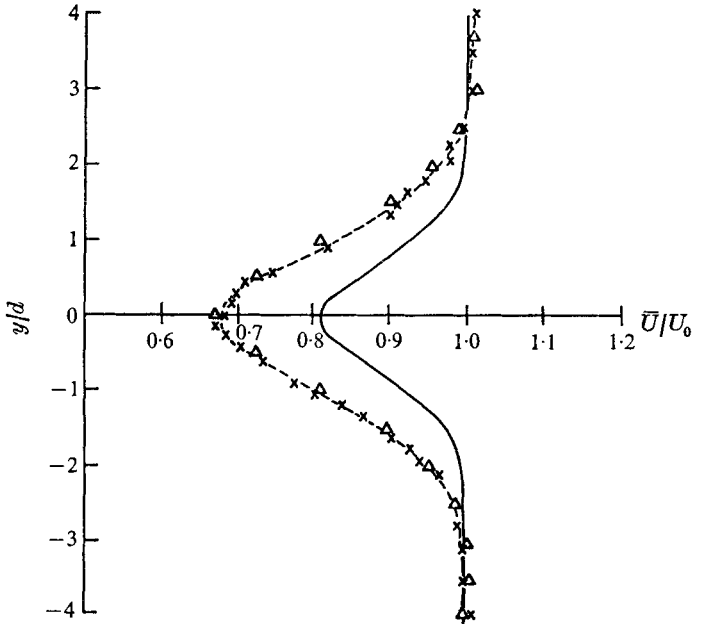

FIGURE 15. Mean velocity profiles in the wake of a stationary D-shape cylinder. —×—, experiment; ——, theoretical model ($\Gamma/U_0 d = 1{\cdot}66$, $R_0/d = 1{\cdot}0$, $b/l = 0{\cdot}21$); △, model prediction plus mean shear from figure 14.

5.3. *Synchronized oscillating* D*-shape cylinder*

The matching process described in §5.2 has been applied to the results obtained in the wake of the oscillating cylinder and the results are presented in figures 10, 11, 16, 17 and 18. It is seen that a considerable mean shear is again required to be superimposed upon the basic arrangement of a street of circular vortices, so that the overall conclusions are essentially the same as for the stationary-cylinder wake. There were, however, certain difficulties in matching details of the measured distributions, especially in the area of the outer core radius, $y/d \sim 2{\cdot}2$. It was suggested earlier that the oscillating body synchronized the phase of vortex production and produced a less variable vortex structure at the measuring position, thus revealing more of the true character in the average shape. It must, therefore, be considered that the deficiency of u velocity energy in figure 16 and the departure from almost perfect symmetry of the defect in figure 17 may be due to inadequacies in modelling the vortices as circular structures. It is also evident from figure 17 that the additional shear adds a significant amount of vorticity at the vortex centre (figure 10), an unnecessary addition in terms of obtaining a good fit. The selection of the vortex parameters is not, however, a completely deterministic process and alternative descriptions could well be possible. The final vortex strength seems an overestimate when compared to the experimental value of 3·24, though it is noted that the choice of a weaker basic vortex street to remedy this would require more adjustment of the vortex

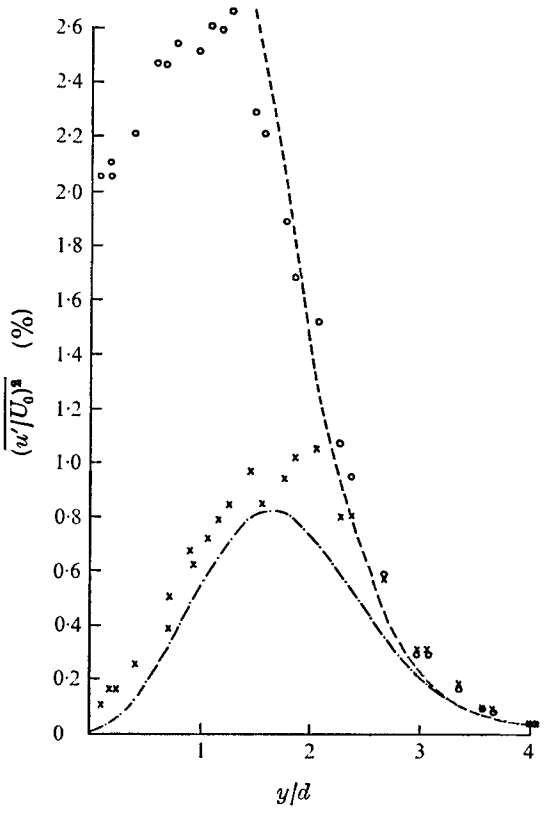

FIGURE 16. Variance of average velocity fluctuations at $x = 8d$ in the wake of an oscillating D-shape cylinder. Experiment ($2a/d = 0{\cdot}4$, $U_n = 8$): ×, u velocity; ○, v velocity. Model predictions: —·—, u velocity; -------, v velocity.

itself to match the energy curve in figure 16. Arguably, this could be more realistic, however, and might underline the need to depart from axisymmetric distributions as a means of description.

6. Conclusions

The technique of conditional averaging has been shown to be useful in examining the conditions in the wake of a stationary and oscillating D-shape cylinder. When the body was oscillated in such a way as to lock the vortex shedding to its own frequency significant changes were observed in the vortex street structure. The cylinder movement was shown to enhance the production of vorticity such that the resultant vortices were found to have 35 % more circulation than those in the stationary-body wake. It was estimated, however, that in both cases only a quarter of the vorticity shed from the front face survived the vortex production process. A vortex model has been constructed to attempt to simplify the vortex street description and this has revealed that a mean shear needs to be added to the basic array of circular vortices for an adequate match of the

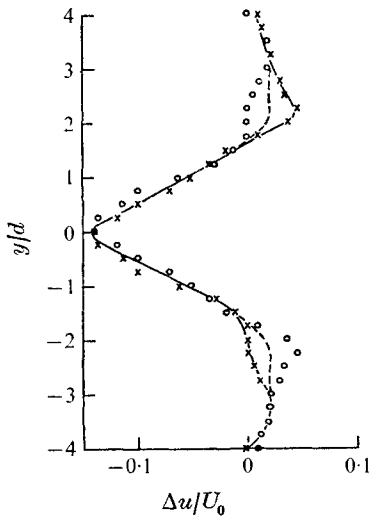

FIGURE 17

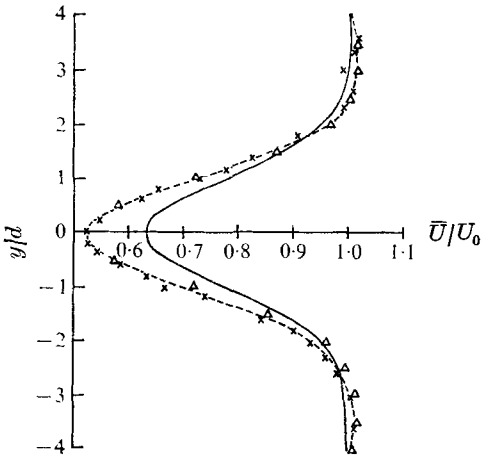

FIGURE 18

FIGURE 17. Oscillating D-shape cylinder ($2a/d = 0{\cdot}4$, $U_n = 8$). Additional velocity required to match theoretical model with experiment. —×—, required velocity through a vortex centre; —○—, inversion of —×— profile; – – – –, mean additional shear.

FIGURE 18. Mean velocity profiles in the wake of an oscillating D-shape cylinder ($2a/d = 0{\cdot}4$, $U = 8$). ×, experiment; ——, theoretical model ($\Gamma/U_0 d = 3{\cdot}67$, $R_0/d = 1{\cdot}45$, $b/l = 0{\cdot}25$); △, model prediction plus additional shear from figure 17.

measured average profiles. In comparing the directly measured wake circulation with estimates inferred from vortex street models, it has become clear that such values are particularly sensitive to their means of determination.

It has been pointed out that the success in using circular vortices to predict the average wake structure is not incompatible with the existence of individual vortex clouds which are non-circular and distort and rotate as they move downstream.

The work reported here was supported by the S.R.C. as part of a programme of basic studies of turbulent flows. The investigation was initiated by Dr P. W. Bearman and I should like to thank him for his subsequent supervision and support.

REFERENCES

BERGER, E. 1964 Die Bestimmung der hydrodynamischen Grössen einen Karmanschen Wirbelstrasse aus Hitzdrahtmessungen bei kleinen Reynoldschen Zahlen. *Z. Flugwiss.* **12**, 41.

BLOOR, M. S. & GERRARD, J. H. 1966 Measurements of turbulent vortices in a cylinder wake. *Proc. Roy. Soc.* A **294**, 319.

CLEMENTS, R. R. 1973 An inviscid model of two-dimensional vortex shedding. *J. Fluid Mech.* **57**, 321.

DAVIES, M. E. 1975 Wakes of oscillating bluff bodies. Ph.D. thesis, University of London.

DWYER, H. A. & MCCROSKEY, W. J. 1973 Oscillating flow over a cylinder at large Reynolds number. *J. Fluid Mech.* **61**, 753.

FAGE, A. & JOHANSEN, F. C. 1927 The flow of air behind an inclined flat plate of infinite span. *Aero. Res. Counc. R. & M.* no. 1104.

FENG, C. C. 1968 The measurement of vortex induced effects in flow past stationary and oscillating circular and D-section cylinders. M.A.Sc. thesis, Department of Mechanical Engineering, University of British Columbia.

FERGUSON, N. & PARKINSON, G. 1967 Surface and wake phenomena of vortex-excited oscillations of bluff cylinders. *Trans. A.S.M.E., J. Engng Indust.* **89**, 831.

GERRARD, J. H. 1966 The mechanics of the formation region of vortices behind bluff bodies. *J. Fluid Mech.* **25**, 401.

GRIFFIN, O. M. 1972*a* The effects of synchronized cylinder vibrations on vortex formation and strength, velocity fluctuations and mean flow. *IUTAM Symp. Flow Induced Structural Vibrations, Karlsruhe*, session E.

GRIFFIN, O. M. 1972*b* Flow near self-excited and forced vibrating circular cylinders. *Trans. A.S.M.E., J. Engng Indust.* **94**, 539.

HARTLEN, R. & CURRIE, I. 1970 A lift-oscillator model for vortex-induced vibrations. *Proc. A.S.C.E., J. Engng Mech.* **96**, 577.

HOFFMAN, E. R. & JOUBERT, P. N. 1963 Turbulent line vortices. *J. Fluid Mech.* **16**, 395.

KADEN, H. 1931 Aufwicklung einer unstabilen Unstetigkeitsfläche. *Ing. Arch.* **2**, 140. (See also *R.A.E. Lib. Trans.* no. 403, 1952.)

KOOPMANN, G. H. 1967 The vortex wakes of vibrating cylinders at low Reynolds numbers. *J. Fluid Mech.* **28**, 501.

NOVAK, M. & TANAKA, H. 1975 Pressure correlations on a vibrating cylinder. *Proc. 4th Int. Conf. Wind Effects on Buildings & Structures, Heathrow, London.*

ROSHKO, A. 1954 On the drag and shedding frequency of two-dimensional bluff bodies. *N.A.C.A. Tech. Note*, no. 3169.

SAFFMAN, P. G. 1973 Structure of turbulent line vortices. *Phys. Fluids*, **16**, 1181.

SARPKAYA, T. 1975 An inviscid model of two-dimensional vortex shedding for transient and asymptotically steady separated flow over an inclined plate. *J. Fluid Mech.* **68**, 109.

SCHAEFFER, J. & ESKINAZI, S. 1959 An analysis of the vortex street generated in a viscous fluid. *J. Fluid Mech.* **6**, 241.

TIMME, A. 1957 Über die Geschwindigkeitsverteilung in Wirbeln. *Ing. Arch.* **25**, 205.

TOEBES, G. H. 1967 *Symp. Wind Effects on Buildings & Structures*, vol. 2, paper 37. Nat. Res. Counc. Can.